Verification of Multi-degree-of-freedom Building Modelling for Seismic Response Prediction based on Microtremor Measurement

Yoshiki Ikeda[*], Masahiro Kurata[**] and Jinzhe Xie[***]

[*]Corresponding author
Disaster Prevention Research Institute, Kyoto University
Address: Gokasho, Uji, Kyoto 611-0011, JAPAN
TEL: +81-774-38-4086, FAX: +81-774-38-4334, E-mail: ikeda.yoshiki.6r@kyoto-u.ac.jp

[**] Disaster Prevention Research Institute, Kyoto University
[***] Graduate School of Engineering, Kyoto University

Abstract

The applicability of the proposed dynamic response model for buildings is investigated using shaking-table tests with a four-storey steel specimen. This approach derives the equation of motion for a multi-degree-of-freedom linear building based on microtremor measurements. Under a linear assumption, the equation can estimate the seismic response accelerations, velocities, and displacements at microtremor sensor locations without the need for information about the mass, damping, stiffness matrices or need for structural design documents to estimate peak responses that are linked with seismic damages of structural and non-structural components. The modelling is unconstrained by structural shape, composition of frames, connections of structural members, or the assumption of a rigid floor. In comparison to the previous methods assuming simple/regular building shape with standard/typical rigid floor, the proposed model is applicable to large-scale low-rise buildings with irregular shapes, flat expanses, and open spaces such as large atria and skylights as well. The applicability study considers two practical scenarios: natural frequencies and damping ratios based on microtremors that can be updated by an earthquake and a standard assumption for structural design. The prediction accuracy is best when the participation vector for seismic input is obtained from sensors located on the upper floors; the structure mostly exhibits elastic response; a modal system identification is applied to the seismic measurement; and local damage does not affect the global seismic response of the structure. The reason is that this method assumes that identified mode shapes do not change due to the occurrence of an earthquake.

KEYWORDS: damage estimation; M-DOF system; microtremor; modal system identification; participation vector for seismic input; seismic response prediction

1. INTRODUCTION

Research interest in the application of vibration monitoring to seismic damage detection for buildings gained popularity in Japan after the 1995 Kobe Earthquake. This earthquake revealed that structural researchers and engineers require a considerable amount of effort and time to evaluate the safety of many buildings immediately after a large earthquake.[1] The 2011 Great Tohoku Earthquake occurred when research and development in this field were underway; after the earthquake it was discovered that instructions to help earthquake victims to return home after the main shock and during the aftershock were confusing in Tokyo.[2] This facilitated the promotion of structural health monitoring in building engineering. Currently, large cities in Japan, e.g., cities around Tokyo, Osaka, Nagoya, and Sendai, recommend that office building users can stay in the building for at least three days if building safety measures are implemented after a large earthquake.[3–5] However, it is impossible for non-experts in structural engineering to guarantee building safety. Therefore, the automation of seismic damage assessment can aid the decision making for building use after an earthquake. This is another reason for the increased interest in damage detection in vibration monitoring.[6]

In practical applications of structural health monitoring, the total number of installed sensors is economically limited in an actual building, and this requires integration of the measurement and analysis to provide building users with useful information about structural damage. Limongelli [7] classifies research approaches employed to estimate the overall structural response under a dynamic excitation with a limited number of recorded responses into four categories: (1) to reduce the total number of DOF (degree-of-freedom) of the structural system by considering system identification results with a limited number of sensors [8–10]; (2) to use the extended Kalman Filter [11, 12]; (3) to expand the measured mode shapes to the total dynamic DOFs [13–15]; and (4) to optimise the sensor locations [16–19]. For a medium-/high-rise steel building, linearly equivalent dynamic properties can be easily evaluated in the lowest vibration modes with a limited number of sensors. It is possible to estimate the structural responses at all floors and in all stories equivalently by modifying some sinusoidal mode shapes based on the identification results.[20] This approach is classified into the third category. The idea was verified by the acceleration measurements that were recorded in the 29-storey steel building in Tokyo during the 2011 Great Tohoku Earthquake.[20] The estimation method has the advantage of conducting seismic response analysis without requiring the mass, damping, and stiffness matrices.[21, 22]

Seismically induced non-structural damage can be classified as acceleration-sensitive phenomenon, drift-sensitive phenomenon, or combined phenomenon.[23–27] Thus, response accelerations, velocities, and displacements on all floors are useful information for making decisions regarding the tentative use of a building immediately after an earthquake. From the floor response, inter-storey displacement can be calculated to obtain damage information, i.e., whether columns, beams, walls, and braces perform nonlinearly or not, and damage possibilities of non-structural components for each storey. Concepts that use sensors on the restricted floors were verified under larger excitations by shaking-table tests on

a 1/3-scale 18-storey test specimen.[28–30] Following Ikeda and Hisada,[20] Hatada *et al*.[28] employed the identified mode shapes; Morii *et al*.[29] employed the mode shapes of the analytical model; and Kodera *et al*.[30] employed the cubic spline interpolation to estimate the responses on all floors directly from a limited number of accelerograms. The estimation does not need system identification based on the accelerograms. Limongelli [7] proposed a response estimation scheme based on cubic spline interpolation. The method expresses the response at each time as a function of floor locations and utilises the functions to estimate the response on the floors without the installed sensors. Limongelli's scheme assumes fixed-end boundary condition at the base of the building and free-end boundary condition at the top of the building; therefore, the building can be expressed as a cantilever beam. Kodera *et al*.[30] removed the cantilever assumption to improve the prediction errors on the floors near the base and the roof. All these approaches are based on modal analysis, which means linearisation in structural dynamics. They assume that sensors such as accelerometers are permanently installed to estimate seismic responses in an objective building. For high correlation with damage, the accuracy of these estimations is within an error of 20 % for the maximum response at each floor.[20, 28–30] Even if the structure performs nonlinearly under a larger earthquake, the modal analysis is a useful tool for tall steel buildings.

The methods proposed in the completed works implicitly assume a simple/regular building shape with the same standard/typical rigid floor.[20, 28–30] This assumption is mostly applicable to high-rise buildings where the vibration characteristics can be expressed through a simple mathematical model. However, the modal identification results of large-scale low-rise buildings indicate that the seismic response estimation methods for high-rise buildings cannot be applied to buildings with irregular shapes, flat expanses, and open spaces such as large atria and skylights.[31]. New estimation approaches are expected in seismic response prediction for low-rise buildings by the private owners and governmental organizations because the number of low-rise buildings is much higher than that of high-rise buildings. Thus, this study attempts to investigate the applicability of a newly proposed response prediction method.

Current building standard seismic codes do not necessarily require vibration analysis for the structural design of low-rise buildings;[32–34] in fact, the vibration measurement of low-rise buildings is rarely conducted. Thus, the dynamic characteristics of these buildings remain unclear compared to those of tall buildings. Besides, it is not economically viable to permanently install many sensors, especially in low-rise buildings, which is another reason the proposed prediction method employs microtremor measurement and modal system identification before performing the dynamic response analysis. Microtremor is an extremely low amplitude ambient vibration caused by ground, man-made, and atmospheric disturbances. Observation of microtremors can give useful information on the dynamic properties of a site or structure, such as the predominant frequencies, damping ratios, and mode shapes. Many practical applications of microtremor to civil engineering structures have been introduced.[35] The proposed method utilises microtremor measurement data to identify natural frequencies, damping ratios, and mode shape vectors at observation points under limited vibration modes. The participation factors in the selected modes are approximated using the corresponding mode shapes for the seismic response analysis.

In this paper, we study the applicability of the proposed structural modelling through shaking-table tests of a 4-storey steel specimen. [21, 22] The modelling involves formulating an equation of motion for a multi-degree-of-freedom (M-DOF) linear building based on microtremor measurements. The advantage is the implementation of the seismic response analysis without information about the mass, damping, and stiffness matrices. That is, the modelling requires no structural design documents for seismic response prediction under a linear assumption. The assumption occurs from the process that the modal properties are determined using microtremor measurements.

The remainder of this manuscript is organised as follows: Section 2 summarises the modelling method for the M-DOF building based on microtremor measurements to study its applicability through the shaking-table tests. Section 3 presents the 4-storey steel structure used as the test specimen. Section 4 describes the modal identification result of the microtremor measurement for making the equation of motion for the corresponding 12-DOF linear structure. Section 5 applies the structural models reported in the previous section to six shaking-table tests wherein the test specimen is excited in linear and nonlinear ranges. Sections 3–5 describe the verification process for the modal system identification using a microtremor for the shaking-table tests. Finally, Section 6 concludes the study.

2. MODELLING OF M-DOF BUILDING BASED ON MICROTREMOR

Ikeda *et al*.[21, 22] have already proposed the basic concept for modelling an equation of motion for an M-DOF linear building based on microtremor measurements. The advantage of this concept is that it can perform seismic response analyses without information about the mass, damping, and stiffness matrices. In other words, the modelling requires no structural design documents for the seismic response prediction under a linear assumption. The design documents include structural calculation sheets, structural calculation process records, and drawings of structure based on the calculation results.

2.1. Modal equation of motion

When an *n*-DOF linear structure with *n* lumped masses is excited by a one-directional horizontal earthquake, the equation of motion is expressed as

$$M\ddot{z}(t) + C\dot{z}(t) + Kz(t) = -Me\ddot{z}_0(t), \tag{1}$$

where M, C, K, e, $z(t)$, and $\ddot{z}_0(t)$ denote the $n\times n$ mass matrix, $n\times n$ damping matrix, $n\times n$ stiffness matrix, n-

dimensional vector for input earthquake (each component is a unit), *n*-dimensional relative displacement vector to the base, and earthquake acceleration input to the structure, respectively. Dot notation implies differentiation with respect to time.

The proposed method assumes that the natural frequencies of the structure can be identified in several lower vibration modes based on microtremor measurements; the corresponding modal amplitudes can be identified at the sensor locations to record the microtremor; and in structural modelling, *n* lumped masses are set at the sensor locations where the modal amplitudes are identified.

The relationship between $z(t)$ and $q(t)$ can be obtained by defining U and $q(t)$ as the *n*×*n* mode shape matrix and the *n*-dimensional modal displacement, respectively, as

$$z(t) = Uq(t) = \begin{bmatrix} u_{11} & u_{12} & \cdots & u_{1n} \\ u_{21} & u_{22} & \cdots & u_{2n} \\ \vdots & \vdots & \ddots & \vdots \\ u_{n1} & u_{n2} & \cdots & u_{nn} \end{bmatrix} \begin{Bmatrix} q_1(t) \\ q_2(t) \\ \vdots \\ q_n(t) \end{Bmatrix}, \tag{2}$$

where $q_j(t)$ denotes the *j*-th modal displacement and u_{ij} denotes the *j*-th modal amplitude at the *i*-th sensor location.

When an undamped eigenvalue problem using the mass and stiffness matrices is considered, and the damping matrix is assumed to be diagonalised by the mode shape matrix, Equation (1) can be decoupled as

$$\begin{Bmatrix} \ddot{q}_1(t) \\ \ddot{q}_2(t) \\ \vdots \\ \ddot{q}_n(t) \end{Bmatrix} + \begin{bmatrix} 2h_1\omega_1 & 0 & \cdots & 0 \\ 0 & 2h_2\omega_2 & \cdots & 0 \\ \vdots & \vdots & \ddots & \vdots \\ 0 & 0 & \cdots & 2h_n\omega_n \end{bmatrix} \begin{Bmatrix} \dot{q}_1(t) \\ \dot{q}_2(t) \\ \vdots \\ \dot{q}_n(t) \end{Bmatrix} + \begin{bmatrix} \omega_1^2 & 0 & \cdots & 0 \\ 0 & \omega_2^2 & \cdots & 0 \\ \vdots & \vdots & \ddots & \vdots \\ 0 & 0 & \cdots & \omega_n^2 \end{bmatrix} \begin{Bmatrix} q_1(t) \\ q_2(t) \\ \vdots \\ q_n(t) \end{Bmatrix} = -\begin{Bmatrix} \beta_1 \\ \beta_2 \\ \vdots \\ \beta_n \end{Bmatrix} \ddot{z}_0(t), \tag{3}$$

wherein

$$[U^T MU]^{-1} U^T CU = \begin{bmatrix} 2h_1\omega_1 & 0 & \cdots & 0 \\ 0 & 2h_2\omega_2 & \cdots & 0 \\ \vdots & \vdots & \ddots & \vdots \\ 0 & 0 & \cdots & 2h_n\omega_n \end{bmatrix}, \tag{4}$$

$$[U^T MU]^{-1} U^T KU = \begin{bmatrix} \omega_1^2 & 0 & \cdots & 0 \\ 0 & \omega_2^2 & \cdots & 0 \\ \vdots & \vdots & \ddots & \vdots \\ 0 & 0 & \cdots & \omega_n^2 \end{bmatrix}, \tag{5}$$

$$[U^T MU]^{-1} U^T Me = U^{-1} Me = b = \begin{Bmatrix} \beta_1 \\ \beta_2 \\ \vdots \\ \beta_n \end{Bmatrix}. \tag{6}$$

In these equations, ω_j, h_j, and β_j denote the *j*-th natural circular frequency, corresponding damping ratio, and *j*-th participation factor for an input earthquake, respectively. β_j expresses the input contribution to the *j*-th modal response of the structure, and b denotes an *n*-dimensional participation vector composed of β_j. Equation (3) can be rewritten as the following scalar equation for the *j*-th mode:

$$\ddot{q}_j(t) + 2h_j\omega_j\dot{q}_j(t) + {\omega_j}^2 q_j(t) = -\beta_j \ddot{z}_0(\mathrm{t}). \tag{7}$$

In general, system identification using microtremors is classified as an output-only identification. The identification cannot evaluate β_j because the factor needs an input-output identification, and the input is unknown/unmeasured because microtremor is an extremely low amplitude ambient vibration caused by ground, man-made, and atmospheric disturbances.

2.2. Approximation of participation vector

The key issue to obtain seismic structural response is evaluating the participation vector by considering a limited number of identified modes because only the lower modes can be identified in practical applications for a building. The limited number of identified modes is denoted by m $(m < n)$.

The modal amplitudes obtained from microtremors are arbitrary, and any amplitude is a relative value to the specified reference amplitude. Further, the participation vector depends on the normalisation of modal amplitudes. The proposed method normalises the *j*-th modal amplitudes such that the sum of amplitude squares becomes unity.

$$u_{1j}^2 + u_{2j}^2 + \cdots + u_{nj}^2 = 1. \tag{8}$$

The participation vector is constrained such that the product of the mode shape matrix and participation vector becomes unity.

$$Ub = \begin{bmatrix} u_{11} & u_{12} & \cdots & u_{1n} \\ u_{21} & u_{22} & \cdots & u_{2n} \\ \vdots & \vdots & \ddots & \vdots \\ u_{n1} & u_{n2} & \cdots & u_{nn} \end{bmatrix} \begin{Bmatrix} \beta_1 \\ \beta_2 \\ \vdots \\ \beta_n \end{Bmatrix} = \begin{Bmatrix} 1 \\ 1 \\ \vdots \\ 1 \end{Bmatrix} \quad (\text{or } \sum_{j=1}^{n} u_{ij}\beta_j = 1). \tag{9}$$

The nondimensional $u_{ij}\beta_j$ is not affected by amplitude normalisation. Considering that limited modes can be identified, Equation (9) should be replaced by

$$\sum_{j=1}^{m} u_{ij}\beta_j = 1 \quad (i = 1,\ 2,\ \cdots\ n). \tag{10}$$

A mode truncation error appears in the modal analysis, especially at the lumped masses nearest the base at which the point is fixed in the *n*-DOF model.[36] When the participation vector is approximated using a limited number of identified modes, it is preferable to select the sensor locations away from base.

By defining $l\ (m \le l < n)$ as the number of selected sensor locations, Equation (10) is changed to

$$\sum_{j=1}^{m} u_{ij}\beta_j = 1 \quad (i = 1,\ 2,\ \cdots\ l). \tag{11}$$

The LSM evidently requires the previous inequality of $m \le l$. Traditionally, the reduction of stiffness matrix is applied to reduce model dimension. However, it cannot be applied to this approach because it does not need any stiffness matrix and the equation of motion has already been uncoupled. In practical applications, the method inevitably checks for an approximation error based on Equation (11): whether the summation on the left side is approximately equal to a unit or not. This check will be implemented by Table 3 in Sub-section 4.2. The corresponding matrix-vector representation is

$$U_{lm}b_m = \begin{bmatrix} u_{11} & u_{12} & \cdots & u_{1m} \\ u_{21} & u_{22} & \cdots & u_{2m} \\ \vdots & \vdots & \ddots & \vdots \\ u_{l1} & u_{l2} & \cdots & u_{lm} \end{bmatrix} \begin{Bmatrix} \beta_1 \\ \beta_2 \\ \vdots \\ \beta_m \end{Bmatrix} = \begin{Bmatrix} 1 \\ 1 \\ \vdots \\ 1 \end{Bmatrix}, \tag{12}$$

where U_{lm} and b_m denote the $l \times m$ mode shape matrix and the *m*-dimensional participation vector, respectively. The subscripts distinguish U_{lm} and b_m from the full-dimensional U and b. The *m*-dimensional participation vector b_m can be obtained using the least squares method (LSM) as

$$\begin{Bmatrix} \beta_1 \\ \beta_2 \\ \vdots \\ \beta_m \end{Bmatrix} = (U_{lm}^T U_{lm})^{-1} U_{lm}^T \begin{Bmatrix} 1 \\ 1 \\ \vdots \\ 1 \end{Bmatrix}. \tag{13}$$

2.3. Seismic response prediction at sensor locations

Equation (7) has three parameters: the *j*-th natural circular frequency, corresponding damping ratio, and *j*-th approximated participation factor. When the input earthquake acceleration is measured at the model base, the acceleration, velocity, and displacement can be obtained in the *j*-th mode. Then, the structural responses at all sensor locations can be obtained by

$$z(t) = \begin{Bmatrix} z_1(t) \\ z_2(t) \\ \vdots \\ z_n(t) \end{Bmatrix} = \begin{bmatrix} u_{11} & u_{12} & \cdots & u_{1m} \\ u_{21} & u_{22} & \cdots & u_{2m} \\ \vdots & \vdots & \ddots & \vdots \\ u_{n1} & u_{n2} & \cdots & u_{nm} \end{bmatrix} \begin{Bmatrix} q_1(t) \\ q_2(t) \\ \vdots \\ q_m(t) \end{Bmatrix} = U_{nm} \begin{Bmatrix} q_1 \\ q_2 \\ \vdots \\ q_m \end{Bmatrix}. \tag{14}$$

In practical applications, natural frequencies and damping ratios in the *m* vibration modes need to be updated from the identified values because they depend on the input excitations and structural response amplitudes. This prediction method assumes that the identified mode shapes do not change during the coming earthquake.

This dynamic modelling is unconstrained by the structural shape, composition of frames, connections of structural members, and the assumption of a rigid floor. The methods proposed in the completed works implicitly assume a simple/regular building shape with the same standard/typical rigid floor.[20, 28–30] This assumption is mostly applicable to high-rise buildings where the vibration characteristics can be expressed through a simple mathematical model. However, the modal identification results of large-scale low-rise buildings indicate that the seismic response estimation methods for high-rise buildings cannot be applied to buildings with irregular shapes, flat expanses, and open spaces such as large atria and skylights.[31] The increasing number of microtremor sensor locations produce a detailed structural model with more lumped masses, which implies that the measurement effort will be rewarded. Under the linear assumption, the modal analysis has the advantage of implementing seismic response analysis without information about the mass, damping, and stiffness matrices.

3. TEST SPECIMEN FOR THE VERIFICATION OF THE PROPOSED METHOD

In December 2020, experimental tests were conducted at a three-dimensional full-scale earthquake testing facility nicknamed 'E-Defense' at the National Research Institute for Earth Science and Disaster Prevention (NIED) near Kobe in Japan. The programme was 'The Tokyo Metropolitan Resilience Project of the National Research Institute for Earth Science and Disaster Resilience: Sub-project C-3'. The project aim was to carry out holistic seismic assessment of critical buildings with due consideration of non-structural components and equipment'.[37] However, shaking tests were planned for other studies and not for the current verification study. The tests were intended to simulate the seismic performance of a hospital, medical equipment, and human bodies on each floor, and a water tank filled with sand was installed on the roof.

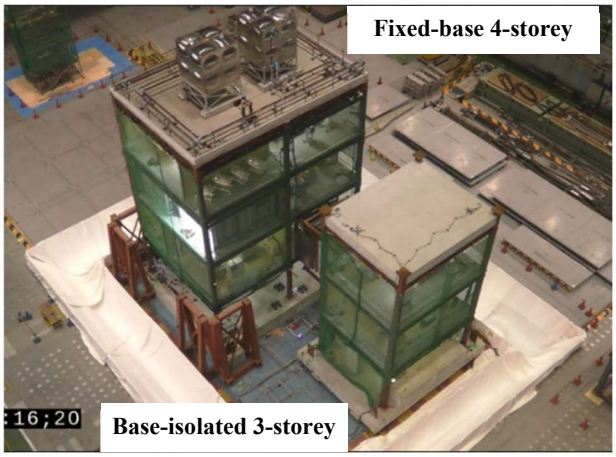

FIGURE 1 Test specimen

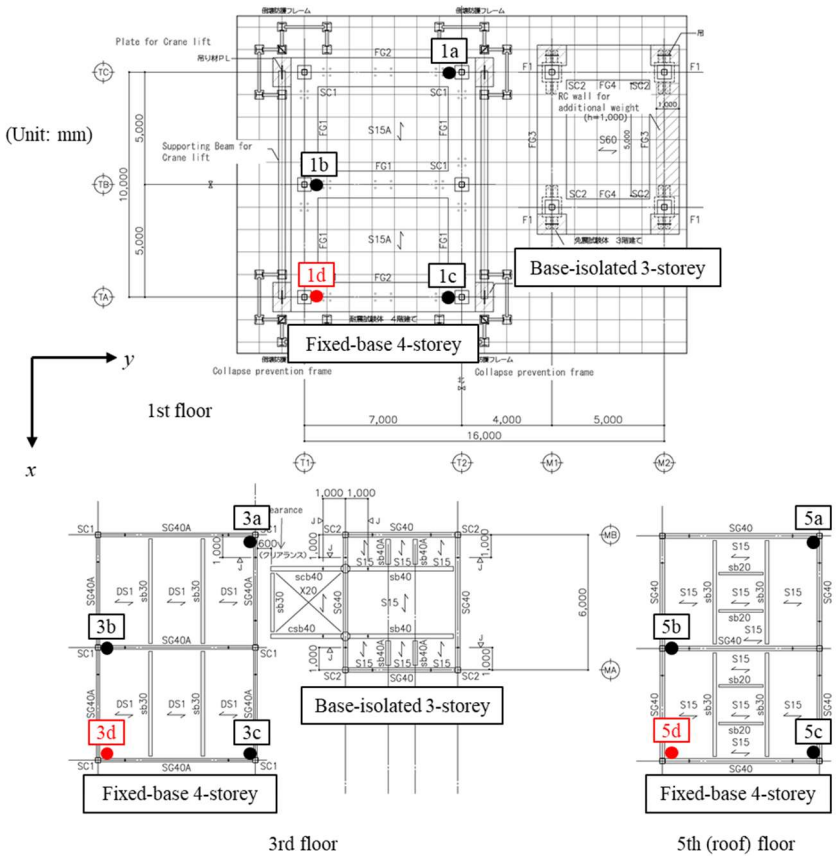

FIGURE 2 Sensor locations on plan views for microtremor measurements

Figures 1 and 2 show the specimens used for the shaking-table tests. Two steel buildings were connected by a bridge with an expansion joint. The 4-storey building was base-fixed, while the 3-storey building was base-isolated. The two buildings were independent of each other in their dynamic behaviour because of the expansion joint. The target building for this study was a base-fixed structure.

The fixed-base building had a 10.0 m (two bays in the *x*-direction) by 7.0 m (one bay in the *y*-direction) floor plan and it was 15.1 m high. The total weight was approximately 3,240 kN, including the concrete foundation. The building's structure was a 4-storey moment-resisting frame designed and constructed according to the current Japanese seismic codes. The frame was composed of steel hollow structural section (HSS) columns and H-shaped steel beams. All column-beam connections had through-diaphragms, and all fixed column bases were designed as the exposed type. All floors were made of 150 mm reinforced concrete slabs on steel deck plates. No claddings were installed; however, the *x*-directional frame was covered with partition walls in the second to fourth stories. The columns were made of 250 × 16 mm cold-rolled HSS BCR295 with a nominal strength of 295 MPa. The main beams were H-shaped (400 × 200 × 8 × 13 mm) made of SN490B steel with a nominal strength of 325 MPa or equivalent built-up steel sections. Floor beams are H-300 × 150 × 6.5 × 19 mm. These column bases are the exposed-type used in Japan, where anchor bolts embedded in the concrete foundation are connected to the base plates welded to the first-storey columns. The column bases are designed to yield prior to the columns, and in turn, the base shear coefficient for the upper structure design is increased by 0.05, according to Japanese specifications.

4. MODAL IDENTIFICATION BASED ON MICROTREMOR

4.1. Microtremor measurements

Before the shaking-table tests, the microtremor of the structure was recorded at 15 locations using five accelerometers. Wireless three-axis accelerometers (M-A351AU by Seiko Epson Corporation, Japan) were used for the microtremor measurements. The amplitude range is ± 5G (G is the gravity acceleration), the average noise density is 0.5 μGrms/√Hz (25 ℃, 0.5–6 Hz, Horizontal ±5 degrees), the peak noise density is 60 μGrms/√Hz (25 ℃, 0.5–100 Hz, Horizontal ±5 degrees), and the resolution is 0.0596 μG/LSB. The radio frequency is in the 920 MHz band and the communication distance is 500 m, when there are no obstacles.

The black spots in Figure 2 show the sensor locations on the first, third, and fifth (roof) floors for the microtremor measurements. The locations on the other floors were horizontally identical to the three floors. For example, Notation ‘5a’ implies sensor location ‘a’ on the fifth floor. Four simultaneous measurements (Measurements A, B, C, and D) were repeated by fixing one accelerometer at Reference location 5a to obtain the global mode shapes of the structure with a limited number of sensors. The reference location was selected on the fifth floor because the modal amplitude might have been relatively larger. The reference location was used to integrate the local mode shapes obtained independently from the four measurements into the global mode shapes of the structure. The proposed method recommends that accelerometers are installed evenly in an objective building to record microtremor responses, because the dynamic nature is unknown *a priori*. In general, the accelerometers are installed as close to the columns as possible to reduce the effect of floor vertical vibration. As illustrated in Figure 2, three sensors were installed on each floor (marked by black spots) and three along vertical lines to measure lateral and torsional vibration modes.

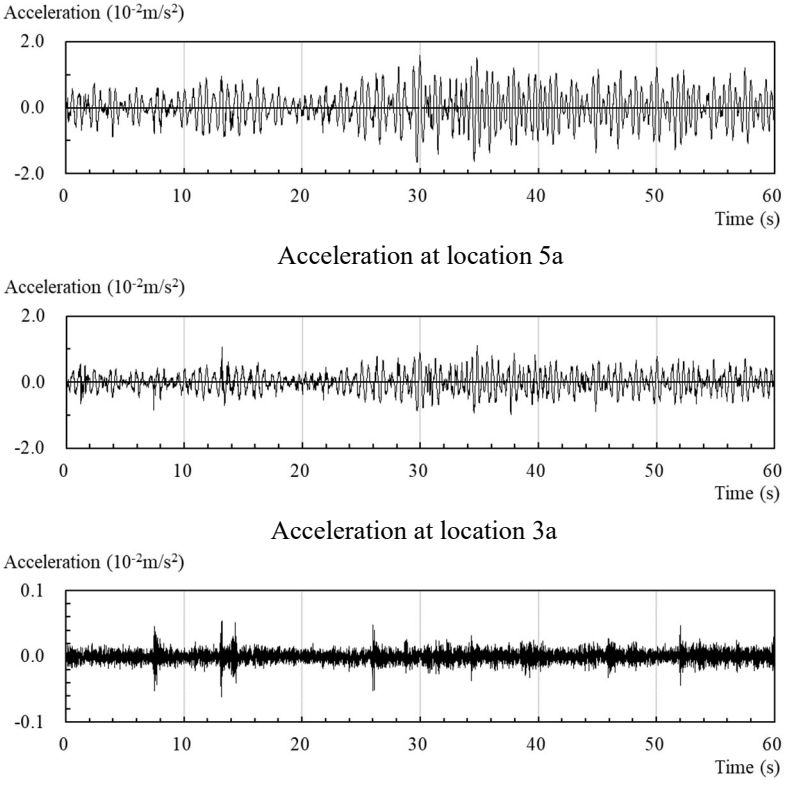

FIGURE 3 *x*-directional microtremor accelerations recorded under Measurement A

Measurement A selected five locations 5a, 4a, 3a, 2a, and 1a on a vertical line, Measurement B selected five locations 5a, 5b, 5c, 4b, and 4c on the upper floors, Measurement C selected five locations 5a, 3b, 3c, 2b, and 2c, and Measurement D selected three locations 5a, 1b, and 1c. The recording length was 25 min for each measurement, and the sampling frequency was 200 Hz. Figure 3 shows the *x*-directional microtremor accelerograms recorded at locations 5a, 3a, and 1a under Measurement A. The peak accelerations were less than 0.02 m/s^2 on the fifth floor and less than 0.006 m/s^2 on the first floor. The sources of vibration are mostly indoor construction activities and ground vibrations, which can be assumed to be random.

4.2. Modal identification results and approximated participation vectors

Natural frequencies and the corresponding mode shapes were identified by the singular value decomposition of power spectra density matrices of outputs in the frequency domain.[38] This modal identification is often called the frequency domain decomposition (FDD) method. The peak frequencies were evaluated as natural frequencies and the corresponding left singular vectors expressed the modal shapes. Its advantage is that it can clearly separate modes located close together, which is particularly useful for a structure with lateral-torsional coupled modes.

Based on the four measurements, Figure 4 shows the distributions of the first singular values in the frequency domain using the FDD method. In one horizontal direction for each measurement, the first singular value distribution was averaged using 20 windows in the time domain. Each window was 40.96 s long, responding to 8192 data sets in the discrete time. Finally, the average distribution curve was smoothed by repeating the Hanning window five times.[39] Averaging and smoothing are useful for identifying natural frequencies more easily by removing the noise included in the microtremor.[31] The peak values on Figure 4 indicate the power levels of each vibration mode. However, these values are relative because the four measurements A, B, C, and D are implemented independently of each other.

Comparing the four distributions of the first singular values in a specific direction, similar peaks appear at slightly different frequencies in the specific frequency bands. Similar peak frequencies were averaged because the maximum difference was 0.1221 Hz at the most around the relatively high frequency of 8.4 Hz. Table 1 lists the natural frequencies selected and averaged from Figure 4. The dominant natural frequencies are 1.57 Hz in the *y*-direction and 1.65 Hz in the *x*-direction. The first torsional frequency is 2.25 Hz. Figure 5 shows the corresponding mode shapes after normalisation to the amplitude at location 5a. Similar to Gentile and Saisi,[40] global mode shapes were obtained using the modal amplitude at Reference location 5a. As indicated in Equation (8), mode shapes are normalised such that the sum of squares of each modal amplitude equals unity for the evaluation of participation factors. Although the second lateral mode in the *x*-direction is alternative either at 4.91 or 5.33 Hz, the first and second modes in the horizontal and torsional directions can be recognised clearly. The damping ratios in the first lateral modes were identified to be 1% by the random decrement method.[41] However, the identified damping ratios were not used in the later verification because the damping ratios under medium/large excitations cannot be estimated by the microtremor.

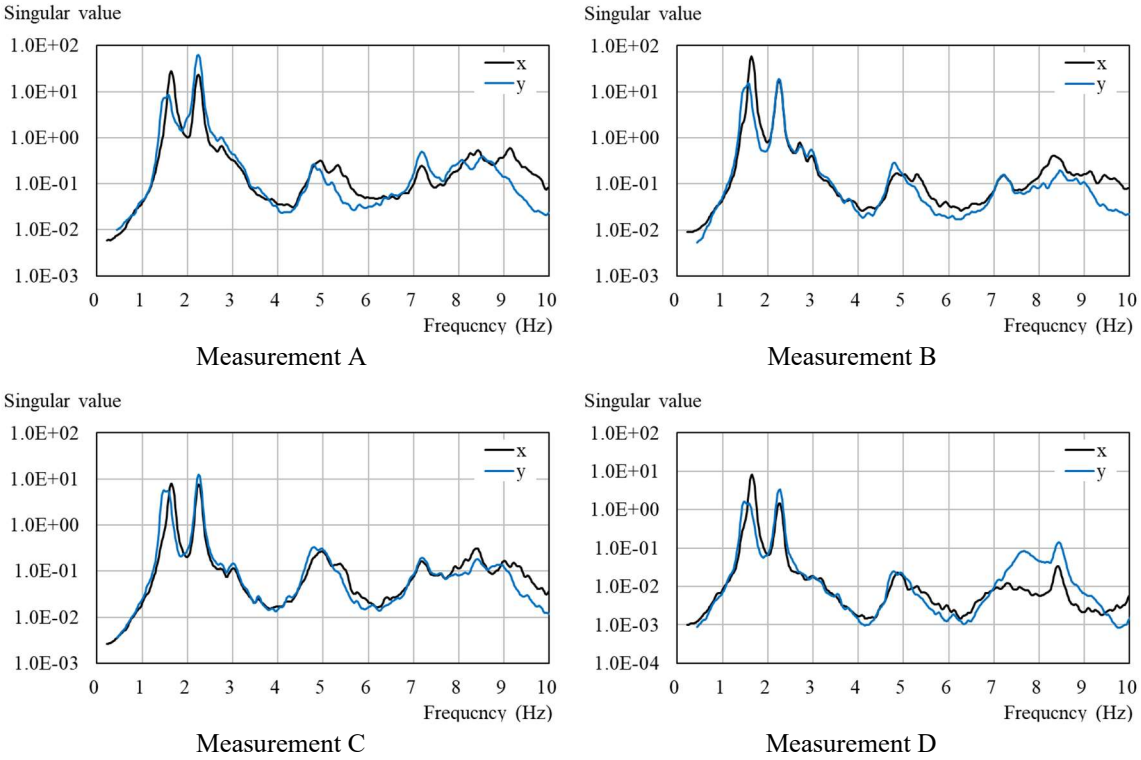

FIGURE 4 Distributions of first singular values by FDD method

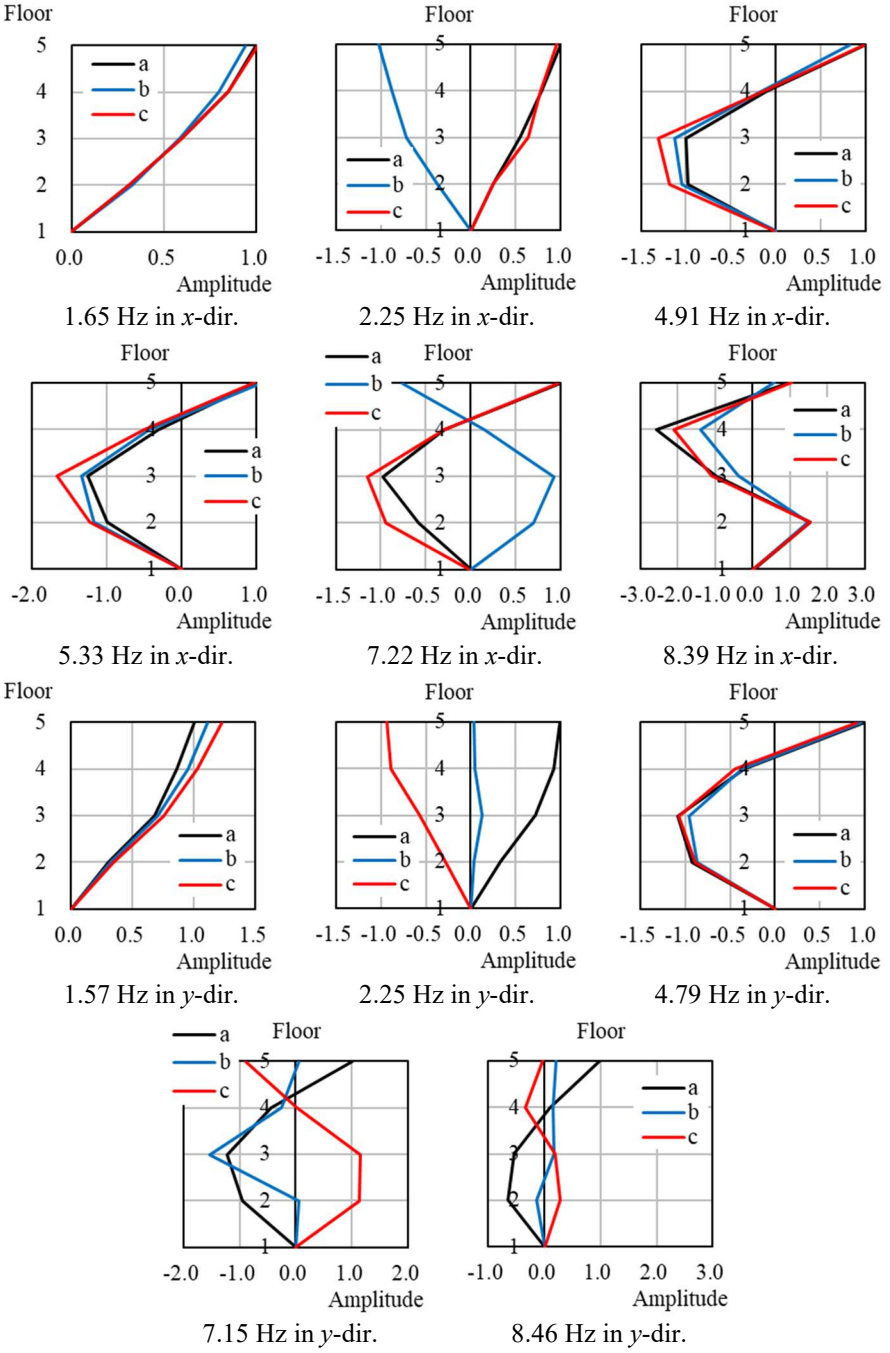

FIGURE 5 Modal shapes

TABLE 1 Natural frequencies identified through microtremor measurements

x-direction		*y*-direction	
Frequency (Hz)	Modal shape	Frequency (Hz)	Modal shape
1.65	Lateral 1st	1.57	Lateral 1st
2.25	Torsional 1st	2.25	Torsional 1st
4.91	Lateral 2nd (Alternative)	4.79	Lateral 2nd
5.33	Lateral 2nd (Alternative)	7.15	Torsional 2nd
7.22	Torsional 2nd	8.46	Not determined
8.39	Lateral 3rd with torsion		

Table 2 indicates the approximated participation factors obtained using both Equation (13) and the mode shapes in Figure 5. Each direction has seven cases in which the considered modes are different from each other because the sensor locations satisfy Equation (11). Cases X-0 and Y-0 satisfy Equation (11) at 12 locations on the second to fifth floors ($l = 12$). Case X-1 satisfied the equation at only nine locations. The total number of identified modes in the *x*-direction is 6. Y-1 satisfies the equation at only five locations in the *y*-direction. The difference in the appointed sensor locations for

Equation (11) is studied in the comparisons of Case X-1 with Cases X-0 and Y-1 with Case Y-0. The effect of the second alternative lateral mode in the *x*-direction is studied by comparing Case X-2 with Case X-3. Various comparisons are listed in Table 2: Cases X-4, X-6, and Y-5 neglect the torsional modes; Cases X-5 and Y-3 consider the lowest three modes; Cases X-6 and Y-5 consider only two lateral modes; and Cases Y-1 and Y-6 study the mode truncation problem depending on the sensor locations described in Sub-Section 2.2.

TABLE 2 Approximated participation factors

Direction	Case	Natural frequencies of considered modes						Sensor locations satisfying Equation (11)
		1.65 Hz	2.25 Hz	4.91 Hz	5.33 Hz	7.22 Hz	8.39 Hz	
	X-0	3.300	0.011	−1.603	0.515	−0.042	0.429	all (12 locations)
	X-1	3.141	−0.024	−1.176	0.390	−0.007	0.095	5a, 5b, 5c, 4a, 4b, 4c, 3a, 3b, 3c
x	X-2	2.086	−0.334	1.127	-	0.370	−0.921	5a, 5b, 5c, 4a, 4b
	X-3	2.271	−0.312	-	0.861	0.452	−0.876	5a, 5b, 5c, 4a, 4b
	X-4	1.567	-	−0.060	1.446	-	-	5a, 5b, 5c
	X-5	1.041	−0.167	2.074	-	-	-	5a, 5b, 5c
	X-6	3.855	-	−1.690	-	-	-	5a, 5b
		Natural frequencies of consider modes						
		1.57 Hz	2.25 Hz	4.79 Hz	7.15 Hz	8.46 Hz		
	Y-0	3.187	0.315	−0.995	0.270	−0.138		all (12 locations)
	Y-1	2.894	0.238	−0.378	0.063	−0.019		5a, 5b, 5c, 4a, 4b
y	Y-2	2.135	0.717	0.536	−0.800	-		5a, 5b, 5c, 4a
	Y-3	1.026	0.032	1.863	-	-		5a, 5b, 5c
	Y-4	2.574	0.219	-	-	-		5a, 5b
	Y-5	0.765	-	2.178	-	-		5a, 5b
	Y-6	−2.178	0.048	−4.377	−0.146	0.398		3a, 3b, 3c, 2a, 2b

TABLE 3 Values on the left side of Equation (10) corresponding to Table 2

Direction	Case	Sensor location												Average
		5a	5b	5c	4a	4b	4c	3a	3b	3c	2a	2b	2c	
	X-0	1.02	1.02	1.04	0.90	0.94	0.93	1.05	1.10	1.14	0.90	0.91	0.97	0.99
	X-1	0.99	1.00	1.01	1.00	0.99	1.00	0.96	1.00	1.03	0.67	0.70	0.72	0.92
	X-2	1.00	1.00	1.00	1.00	1.00	0.90	0.12	0.37	−0.01	-0.33	−0.24	−0.61	Not evaluated
x	X-3	1.00	1.00	1.00	1.00	1.00	0.87	0.19	0.52	0.07	-0.36	−0.08	−0.47	Not evaluated
	X-4	1.00	1.00	1.00	0.41	0.33	0.33	−0.10	−0.14	−0.26	-0.18	−0.24	−0.28	Not evaluated
	X-5	1.00	1.00	1.00	0.24	0.28	0.21	−0.44	−0.44	−0.65	-0.53	−0.52	−0.66	Not evaluated
	X-6	1.00	1.00	1.02	1.35	1.31	1.36	1.45	1.49	1.61	0.99	1.06	1.10	1.23
	Y-0	0.92	0.90	0.84	1.15	1.14	1.19	1.16	0.96	1.20	0.67	0.67	0.70	0.96
	Y-1	1.00	1.00	1.00	1.00	1.00	0.99	0.88	0.81	0.85	0.45	0.44	0.44	0.82
	Y-2	1.00	1.00	1.00	1.00	0.72	0.38	0.87	0.79	−0.13	0.42	0.07	−0.30	Not evaluated
y	Y-3	1.00	1.00	1.00	0.11	0.11	0.08	−0.42	−0.34	-0.41	-0.46	-0.43	−0.44	Not evaluated
	Y-4	1.00	1.00	1.01	0.86	0.86	0.83	0.68	0.64	0.62	0.30	0.29	0.28	0.70
	Y-5	1.00	1.00	1.00	−0.02	−0.02	−0.05	-0.61	−0.51	−0.59	-0.59	−0.55	−0.56	Not evaluated
	Y-6	−1.98	−2.20	−2.27	−0.09	−0.12	-0.24	1.00	1.00	1.00	1.00	1.00	1.07	Not evaluated

Table 3 investigates how the locations satisfy Equation (10) via averages in the right column. Cases X-0, X-1 and Y-0 obtain the participation vectors using the LSM, which means that many locations want to approximately satisfy Equation (10). In each of the other cases, the appointed locations strictly satisfy Equation (11), which means 1.00. Besides Cases X-0 and Y-6, lower values appeared in the lower floors. This implies that mode truncation errors appear at the lumped masses near the base.[36] It would be better to select the sensor locations far from the base to approximate the participation vector under a limited number of identified modes. Cases X-0 and Y-0 may overestimate the seismic responses on the third and the fourth floors, respectively. Cases X-2, and X-3 have similar values, which implies that the selection of the second lateral modes is not significant in the seismic response prediction. Cases X-2, X-3, X-4, X-5, Y-2, Y-3, Y-5, and Y-6 cannot be selected for structural modelling because of the negative values. Case X-6 overestimates the responses on the second to fourth floors because the sums are more than 1.00. Case Y-4 has a small average value.

Thus, Cases X-0, X-1, Y-0, and Y-1 are selected as the candidate models for the seismic response predictions.

5. VERIFICATION WITH THE SHAKING-TABLE TESTS

5.1. Input excitations to shaking table

Table 4 lists the input motions using the shaking table. The tests used two kinds of seismic excitations. The NS-component

of the JMA Kobe-wave was adopted as the earthquake ground motion for simulating hospital damage by an active fault directly beneath the Tokyo metropolitan area. This wave is often used as a short-period and impulsive earthquake for structural design in Japan. The other ground motion (OS2) is an artificial ground motion used to evaluate the seismic damage of relatively long-period contents in hospital buildings and the behaviour of seismic base-isolated buildings. OS2 is a ground motion prepared by the Ministry of Land Infrastructure Transport and Tourism, Japan, for the engineering bedrock in the Osaka region for a mega subduction-zone earthquake along the Nankai Trough. Here, 'OS' stands for Osaka, and '2' stands for the relatively soft ground in the area. The bedrock ground motion was amplified to obtain a ground surface motion considering Type 2 soil conditions (normal stiffness). Then, the ground motions were scaled down to simulate the elastic limit corresponding to the allowable stress design (Level 1: Tests 1, 2 and 3) and the inelastic limit corresponding to the ultimate strength design (Level 2: Tests 4, 5 and 6) in the Japanese seismic design. Tests 1 to 4 excited the objective structure in either the *x*-direction or the *y*-direction to simplify the structural performance. Tests 5 and 6 excited it in both the *x*-direction and the *y*-direction to understand damage of corner columns in the first story well. White noise excitations were input to the structure before and after each earthquake excitation. However, this study did not use the white noise excitations.

TABLE 4 Shaking-table tests

Test sequential No.	Earthquake name	Input direction		Input scale		Peak acceleration on 1st floor (10^{-2}m/s^2)	
		x-dir.	*y*-dir.	*x*-dir.	*y*-dir.	*x*-dir.	*y*-dir.
1	Kobe	Input	-	16%	-	137	16
2	Kobe	-	Input	-	16%	34	149
3	OS2	-	Input	-	20%	22	89
4	Kobe	Input	-	50%	-	406	76
5	OS2	Input	Input	50%	50%	225	207
6	Kobe	Input	Input	50%	50%	544	474

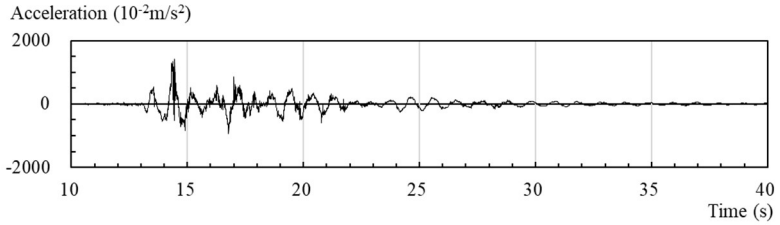

5th floor

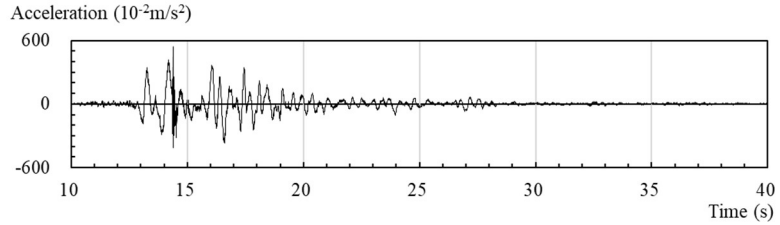

1st floor

(a) *x*-direction

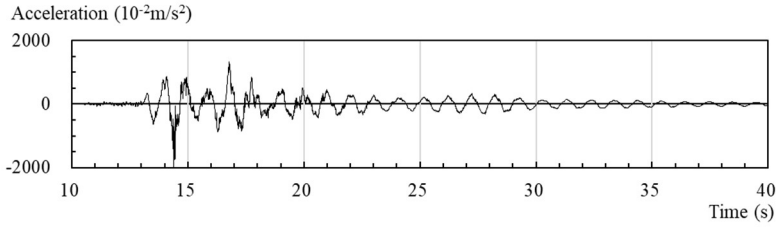

5th floor

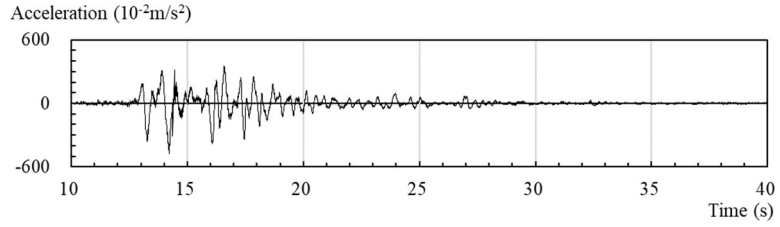

1st floor

(b) *y*-direction

FIGURE 6 Measured accelerograms when the 50%-scale Kobe earthquake is input in two horizontal directions

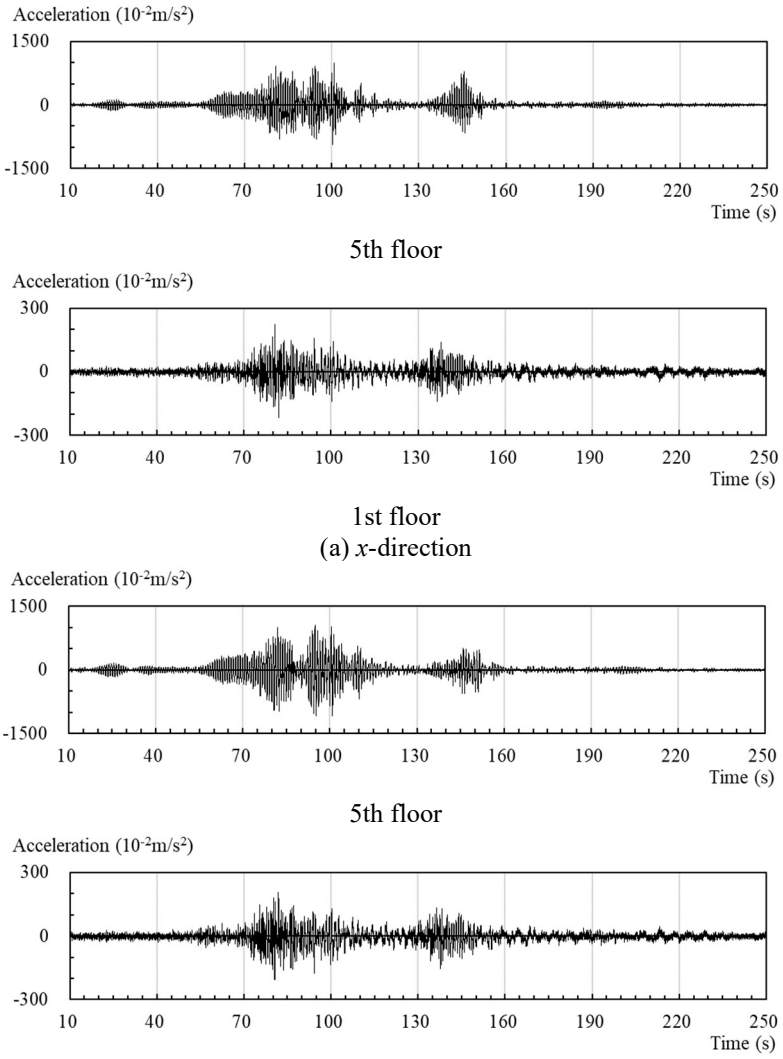

FIGURE 7 Measured accelerograms when the 50%-scale OS2 earthquake is input in two horizontal directions

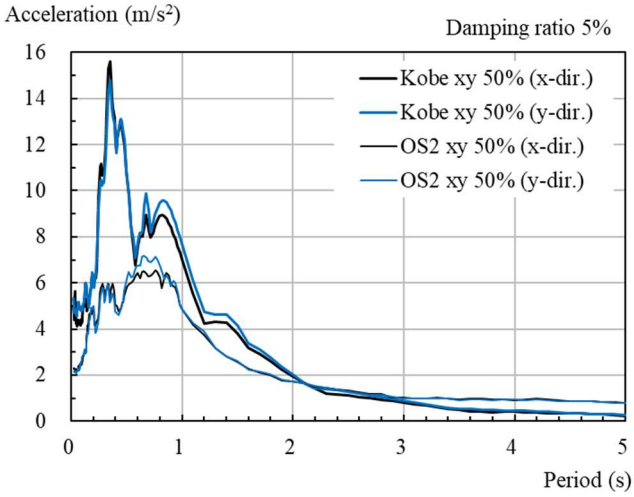

FIGURE 8 Acceleration response spectra of input accelerations on the shaking table

The shaking sequence is the (1 and 2) JMA Kobe motion in a single horizontal direction for a Level 1 design check, (3) small OS2 in a single horizontal direction for evaluating the immediate functionality limit, (4) JMA Kobe motion in a single horizontal direction for Level 2 design check, (5) significant OS2 motion in two horizontal directions for evaluating the functionality limit, and (6) JMA Kobe motions in two horizontal directions with a vertical motion to

evaluate the failure mechanism. The sequential numbers are listed in Tables 4, 5, and 6.

Figure 6 and 7 show the measured accelerograms when the 50%-scale Kobe earthquake is input in two horizontal directions and the 50%-scale OS2 earthquake is input in two horizontal directions. Figures 6 (a) and 7 (a) show the *x*-directional accelerograms, and Figures 6 (b) and 7 (b) show the *y*-directional accelerograms. In each of the last two tests (5 and 6), the *y*-directional input was the same as the *x*-directional input. Figure 8 shows the same input as the acceleration response spectra. In the Kobe earthquake, the maximum input acceleration was approximately 5.0 m/s^2. Several anchor bolts' fractures caused the intense shaking at 14.3 s at the column bases.

In the OS2 earthquake input, the maximum acceleration input was approximately 2.0 m/s^2. However, if we compare the response spectra of the two motions, the spectral acceleration around 0.7–0.8 s, which corresponds to the natural period of the structure, differs only 30%. Figure 9 shows the *x*-directional accelerograms with extreme peak amplitudes under the 50%-scale Kobe earthquake input, Test 6. These recorded the impact movements of the non-structural components indoors.

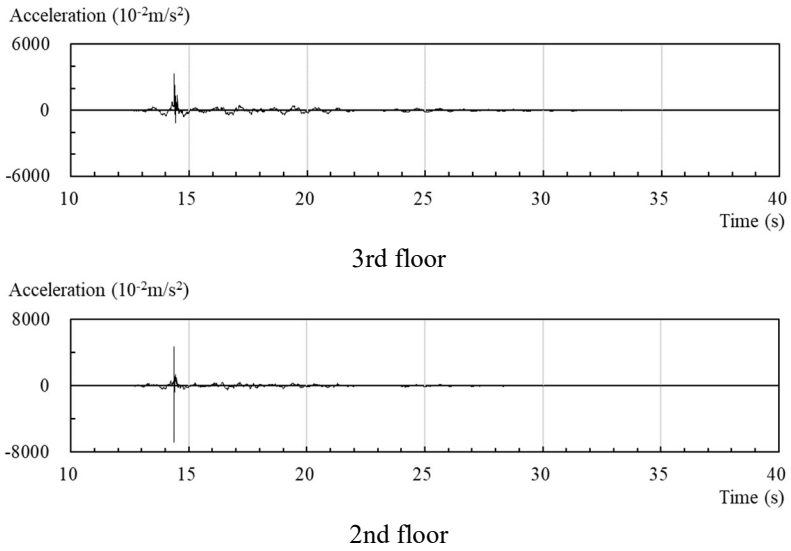

FIGURE 9 *x*-directional accelerograms with extreme peak amplitudes with when the 50%-scale Kobe earthquake is input in two horizontal directions

5.2. Modal identification by recursive LSM method

Modal identification using the recursive LSM method with a forgetting factor [42, 43] was employed to the recorded accelerations to understand the dynamic performance of the nonlinear structure. Five accelerometers located at 1d, 2d, 3d, 4d, and 5d (1d, 3d, and 5d are the red spots in Figure 2) recorded the responses on the shaking-table tests. The identification models are single-input and four-output Auto-Regressive Exogeneous (ARX) models: the input is the acceleration at sensor location 1d, and the outputs are the accelerations at the other sensor locations. The forgetting factor was set at 0.998 to globally determine the time variances of the first equivalent modal properties, i.e., nonlinearity and amplitude dependency. Before the identification, the measured accelerations were bandpass-filtered with the band from 0.5 to 2.0 Hz to fix the dimension for the ARX models to (2,2): the first 2 indicates two auto-regressive terms and the second 2 indicates three exogeneous input terms with the direct term (present term). The identification was conducted in the horizontal direction independent of the other direction. A similar identification has already been applied to the past E-defence tests to understand the structural amplitude-dependency.[44] Reference 44 showed that the identified equivalently-linear properties such as natural frequencies and modal damping ratios have consistency with nonlinear hysteresis curves of a steel structure.

Figure 10 compares time variances in the *x*-direction of the first lateral mode under Kobe excitation tests Nos.1, 4, and 6 in Table 4. The initial 10 s were neglected because of the warm-up period for the shaking. Remarkable variances can be seen in the first 5 s (10 s to 15 s in the figure) when the excitation amplitude becomes extremely large. A negative damping ratio of approximately 13.5 s implies that the ARX model cannot understand the corresponding physical phenomena with causality. Figure 11 compares them under OS2 excitation test Nos. 3 and 6. The natural frequency tended to decrease as the excitation scale increased. The damping ratio increased under the Kobe excitations. Table 5 compares the identified modal properties that were averaged in the 30 s from 10 to 40 s under the Kobe excitations and in 240 s from 10 to 250 s under the OS2 excitations. The positive values were evaluated as zero when the damping ratios were averaged.

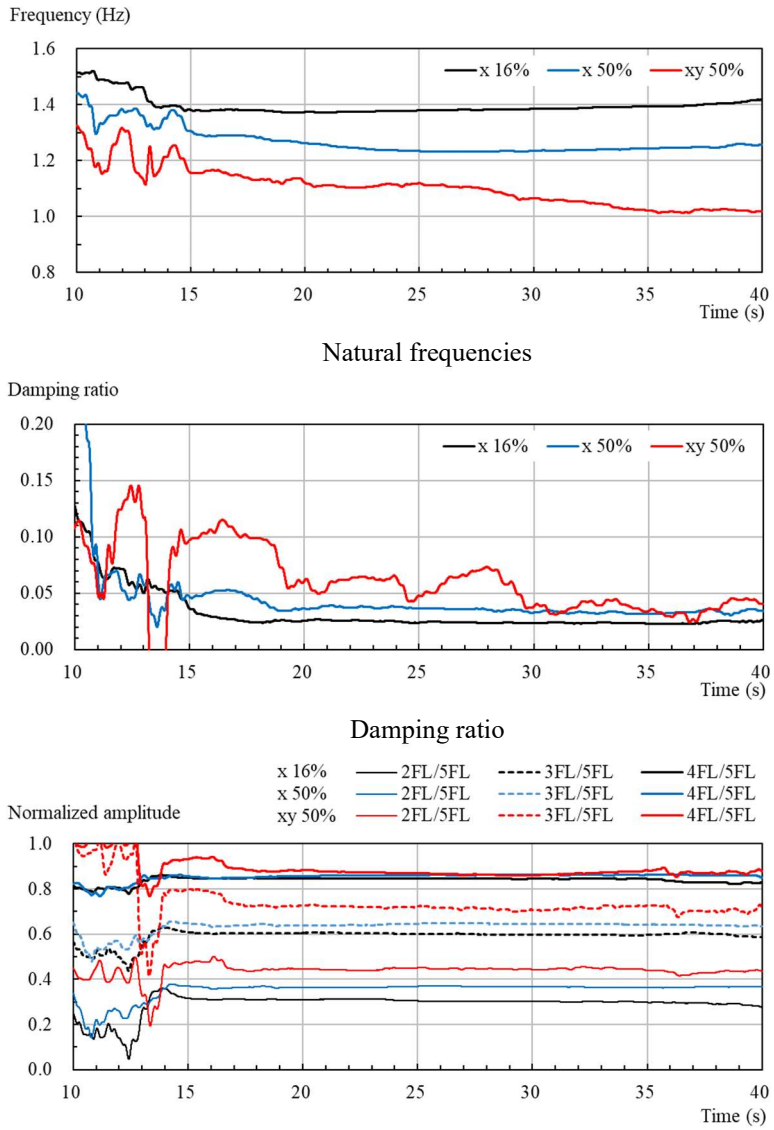

FIGURE 10 Changes of the first modal properties in the *x*-direction under the Kobe excitations

The modal amplitudes were normalised to the amplitude on the fifth floor. The amplitude on the second floor tends to increase after the excitation scale becomes larger, which is a recognised physical phenomenon in which the structural damages were found around the column bases; the damage apparently softened the stiffness in the first storey. The hysteresis relationship of the column bases shows a ratcheting behaviour where anchor bolts yielded in tension do not resist force until the deformation demand exceeds the experienced maximum deformation. The yielded anchor bolts were retightened after shaking. The modal amplitudes at the second and third floors gradually become larger in response to the repetitions of the shaking-table tests with an increase in excitation scales. The assumption that the identified mode shapes are constant may imply a certain limitation in practical applications.

5.3. Verification of proposed method

The applicability of the proposed method is studied by first updating the natural frequencies and damping ratios obtained from microtremors with those obtained from the shaking-table tests. The method then utilises the same modal shapes based on the theoretical assumption. The first applicability test images verify that (1) an instrumented building has an observation system to record at least an input acceleration at the base and an output response on a certain floor in each horizontal direction, (2) modal system identification was applied to the records, and (3) seismic response prediction was expected on the other floors that were not instrumented. Although the verifications are examined in only one horizontal direction, the response prediction results include the effect of torsional vibration. The reasons are, the FDD method can identify lateral modes, torsional modes, and the lateral-torsional coupling modes using one directional microtremor, and that Tests 5 and 6 excited the specimen in two directions. Consequently, the effect of torsional vibration was relatively small in the test specimen, which can be confirmed by the fact that the approximated participation factors in the torsional modes are smaller than ones in the lateral modes in Table 2.

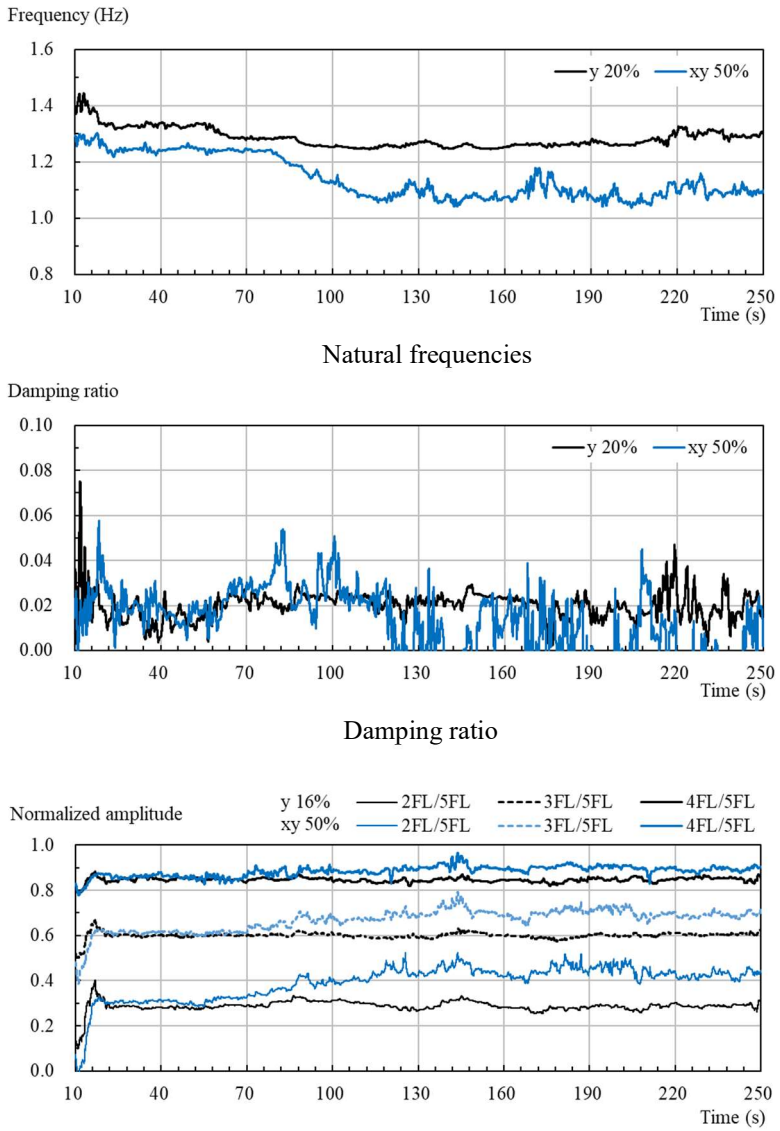

FIGURE 11 Changes of the first modal properties in the *y*-direction under the OS2 excitations

TABLE 5 Comparison of averaged identified modal properties

Direction			Natural frequency (Hz)	Damping ratio (%)	Modal amplitude normalised to 5th floor				Averaging time
					2	3	4	5	
x	Microtremor		1.65	1.0	0.32	0.60	0.84	1.00	
	Sequential shaking No. in Table 4	1	1.40	3.2	0.29	0.59	0.84	1.00	10–40 s
		2	Not identified under *y*-dir. excitation						
		3	Not identified under *y*-dir. excitation						
		4	1.27	4.4	0.35	0.63	0.85	1.00	10–40 s
		5	1.20	4.2	0.38	0.66	0.86	1.00	10–250 s
		6	1.11	6.1	0.44	0.74	0.89	1.00	10–40 s
y	Microtremor		1.57	1.0	0.29	0.64	0.85	1.00	
	Sequential shaking No. in Table 4	1	Not identified under *x*-dir. excitation						
		2	1.30	3.0	0.25	0.58	0.84	1.00	10–40 s
		3	1.28	2.0	0.29	0.60	0.85	1.00	10–250 s
		4	Not identified under *x*-dir. excitation						
		5	1.14	2.0	0.39	0.67	0.88	1.00	10–250 s
		6	1.04	3.9	0.48	0.67	0.88	1.00	10–40 s

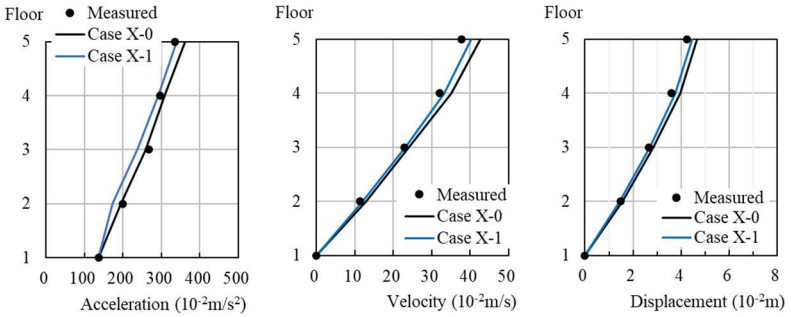

(a) *x*-directional responses under an *x*-directional 16% excitation

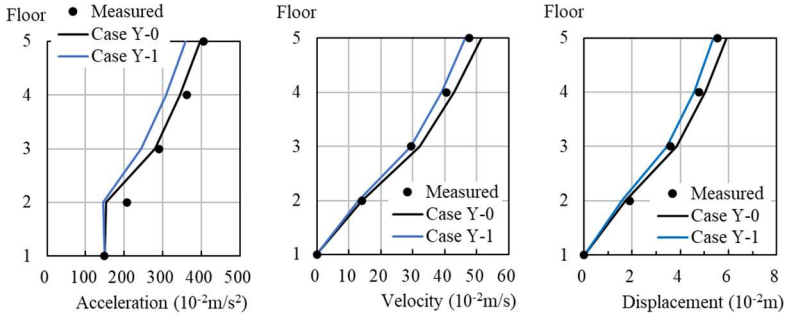

(b) *y*-directional responses under a *y*-directional 16% excitation

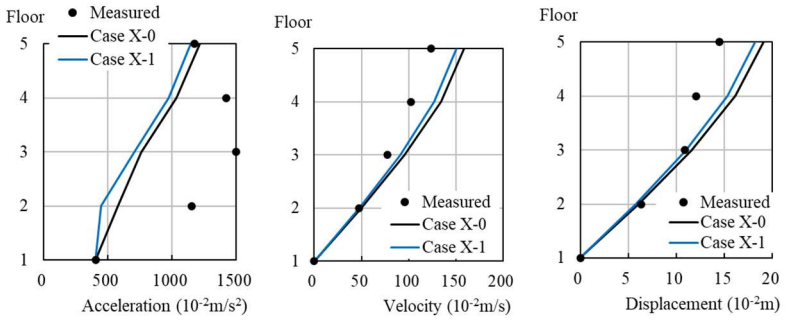

(c) *x*-directional responses under an *x*-directional 50% excitation

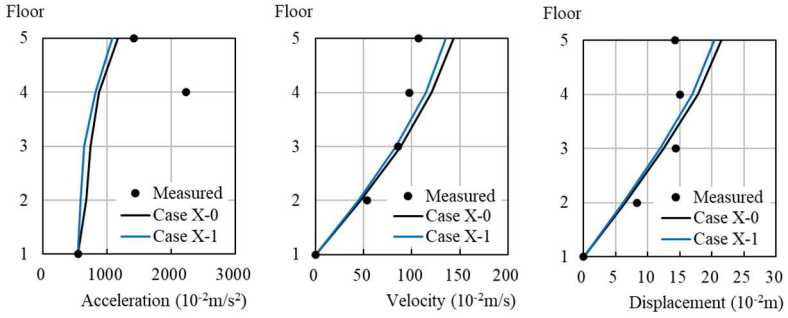

(d) *x*-directional responses under *x*- and *y*-directional 50% excitations

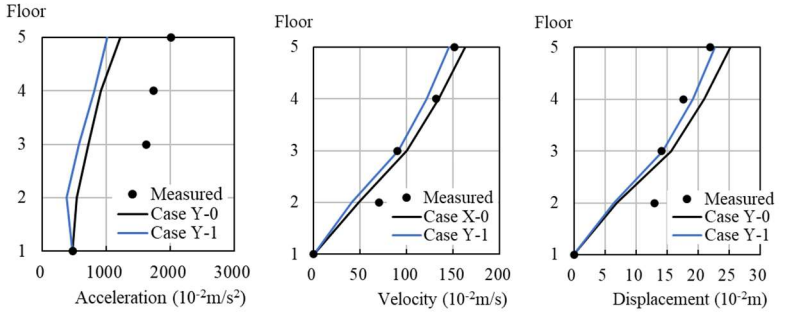

(e) *y*-directional responses under *x*- and *y*- directional 50% excitations

FIGURE 12 Measured and predicted peak responses under the Kobe Earthquake, considering averaged identified modal properties

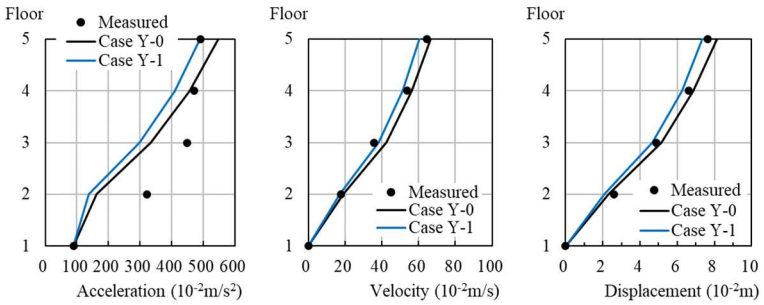

(a) *y*-directional responses under a *y*-directional 20% excitation

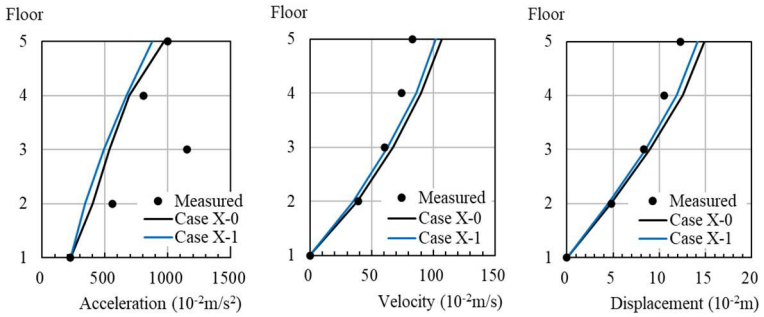

(b) *x*-directional responses under *x*- and *y*-directional 50% excitations

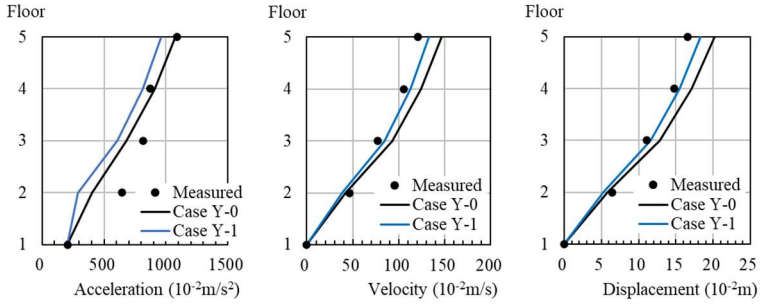

(c) *y*-directional response under *x*- and *y*-directional 50% excitations

FIGURE 13 Measured and predicted peak responses under the OS2 Earthquake, considering averaged identified modal properties

In each verification using the shaking-table test, an equivalently linear model has the average natural frequency for the first lateral mode, decreases the natural frequencies for the other modes with the same frequency ratios in the first lateral mode, and utilises the same damping ratio in the first lateral mode for all modes. Figure 5 and Table 5 indicate that this model determines all parameters for each model. Cases X-0, X-1, Y-0, and Y-1 are candidate models for seismic response prediction. The velocities and displacements relative to the first floor were obtained by integrating the accelerations recorded at locations 1d, 2d, 3d, 4d, and 5d to compare the predicted seismic responses with the corresponding measurements.

Figure 12 compares the predicted peak responses with the corresponding measurements under the Kobe excitations and Figure 13 compares them under the OS2 excitations. Figures 12 (a), 12 (b) and 13 (a) show the responses under the Level 1 shaking Nos. 1, 2 and 3, respectively. Figures 12 (c), 12 (d), 12 (e), 13(b) and 13 (c) show the responses under the Level 2 shaking Nos.4, 5 and 6. In these figures, the predicted response on a certain floor is the average value of the three responses at the microtremor sensor locations on the same floor. Comparisons of accelerations under the 50%-scale excitations are impossible because the extreme peak values on some floors, as shown in Figure 9, were recorded by the impact movements of the non-structural components indoors. Cases X-0 and Y-0 estimate the seismic responses larger than Cases X-1 and Y-1, respectively. The applied method is most useful under the 16%-scale Kobe and the 20%-scale OS2 excitations because of the linear assumption. The stiffness softening in the first storey makes it difficult to predict the seismic responses under 50%-scale excitations. However, the prediction accuracy is better under the 50%-scale OS2 excitation than that under the 50%-scale Kobe excitation.

The next verification test considers the practical scenario in which a building observes only an input acceleration at the base. Now, the test assumes two cases: (1) use 85% values of all natural frequencies identified through the microtremor and stiffness-proportional damping matrix (i.e., frequency-proportional damping matrix, or internal viscous damping matrix) with a 2% damping ratio in the first lateral mode; and (2) use 70% values of all natural frequencies identified through the microtremor and stiffness-proportional damping matrix with a 3% damping ratio in the first lateral mode.

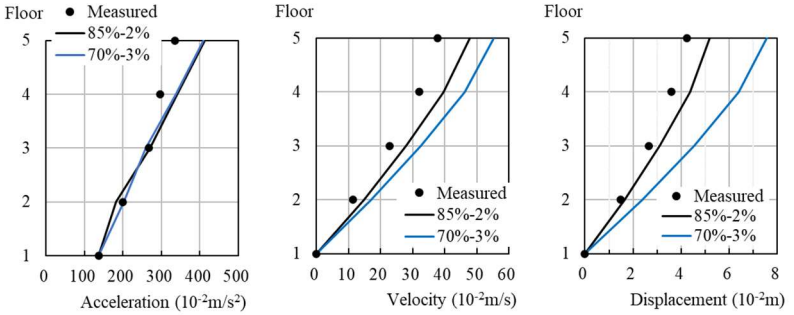

(a) *x*-directional responses under an *x*-directional 16% excitation

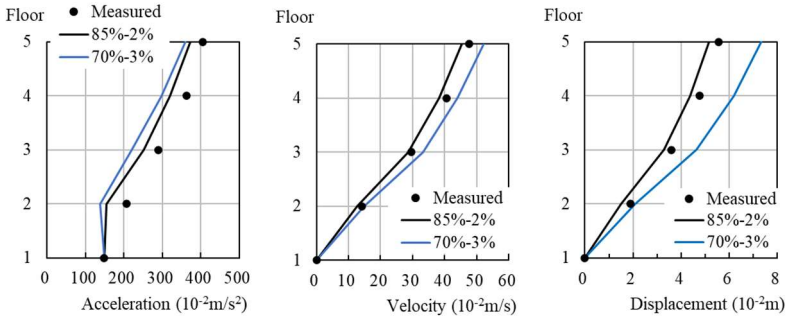

(b) *y*-directional responses under a *y*-directional 16% excitation

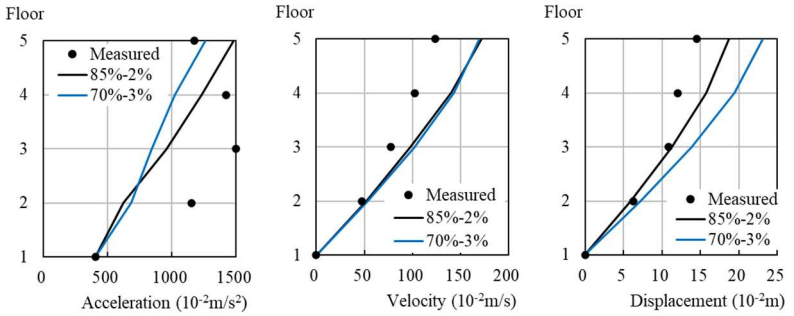

(c) *x*-directional responses under an *x*-directional 50% excitation

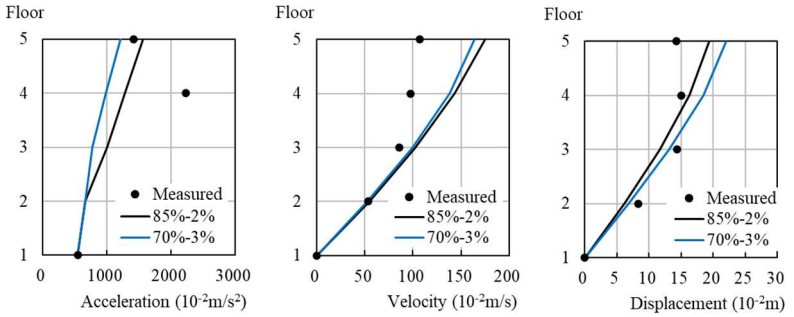

(d) *x*-directional responses under *x*- and *y*-directional 50% excitations

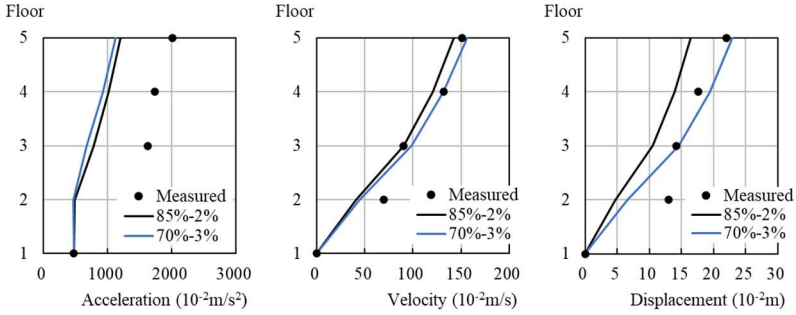

(e) *y*-directional responses under *x*- and *y*- directional 50% excitations

FIGURE 14 Measured and predicted peak responses under the Kobe Earthquake, considering design scenario

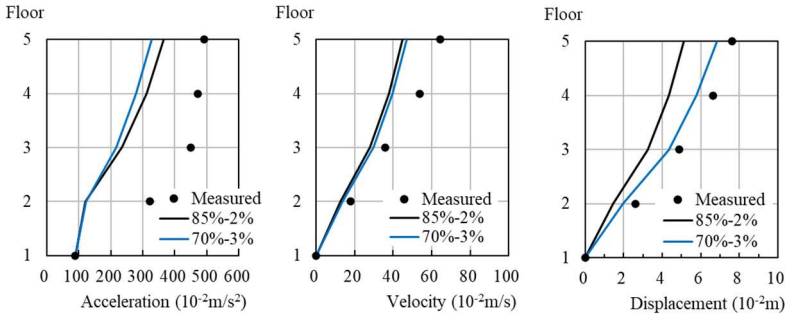

(a) *y*-directional responses under a *y*-directional 20% excitation

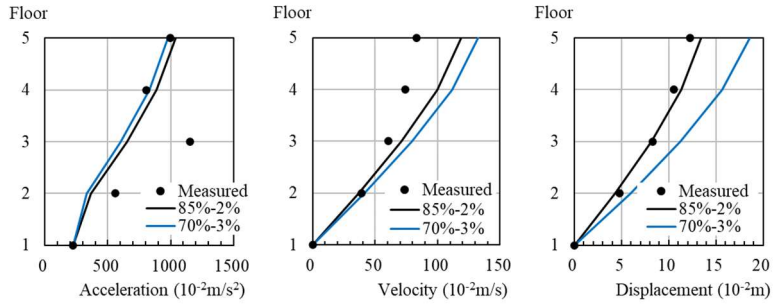

(b) *x*-directional responses under *x*- and *y*-directional 50% excitations

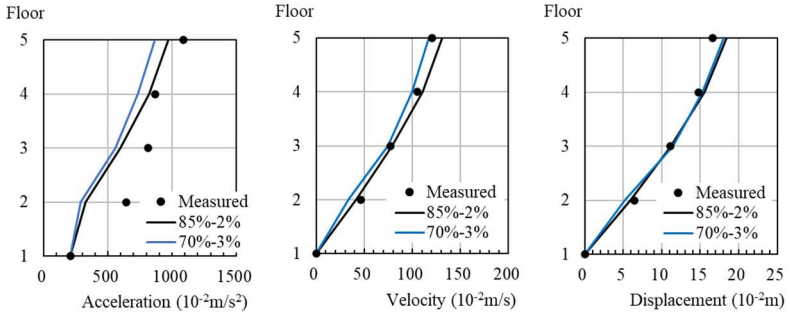

(c) *y*-directional response under *x*- and *y*-directional 50% excitations

FIGURE 15 Measured and predicted peak responses under the OS2 Earthquake, considering design scenario

Generally, dynamic properties are different under microtremor and earthquake level even when there is no obvious structural damage. For reference, the comparison of microtremor records and the seismic records in six tall buildings reveal that the decrease of the first natural frequency is generally 10 to 20% in steel structures and 20 to 30% in reinforced concrete structures.[45–51] The comparison of pre-shock and main shock records after the 2011 Great Tohoku Earthquake revealed a 10% decrease found in two other tall steel buildings in Tokyo.[52] These reports led to 85 and 70% values in changing the natural frequencies. However, damping ratios has more variances than the natural frequencies.

Figures 14 and 15 compare the two cases with the experimental records: the latter case with the lower frequencies and higher damping ratios (Notation 70–3% in the figures) images indicate that the structure is more excited than the former case (Notation: 85–2%). Similar to Figures 12 and 13, Figures 14 (a), 14 (b) and 15 (a) show the responses under the Level 1 shaking Nos. 1, 2 and 3, respectively. Figures 14 (c), 14 (d), 14 (e), 15(b) and 15 (c) show the responses under the Level 2 shaking Nos.4, 5 and 6. The structural design in Japan often assumes a stiffness-proportional damping matrix with a value of 2% in the first lateral mode for steel structures. For reference, five identified large-scale low-rise commercial buildings show that the first natural frequencies assumed at structural designs were approximately 65–80% values under the microtremor.[31] The two cases in Figures 14 and 15 adopt Cases X-1 and Y-1 for the participation vector because the small differences between two cases (Cases X-0 and X-1 in *x*-direction; Cases Y-0 and Y-1 in *y*-direction) are found in the seismic response prediction, as shown in Figures 12 and 13.

Before comparing Figures 12 to 15, note that 85% of the first natural frequency is 1.41 Hz in the *x*-direction, and it is approximately equal to 1.40 Hz under the *x*-directional 16%-scale Kobe excitation in Table 5. Similarly, 85% of the first natural frequency is 1.34 Hz and it is nearly equal to 1.30 Hz under the *y*-directional 16%-scale Kobe excitation. In the *x*-direction, the 70% natural frequency is 1.16 Hz and it is nearly equal to 1.20 Hz under the bidirectional 50%-scale OS2 excitation and 1.11 Hz under the bidirectional 50%-scale Kobe excitation. In the *y*-direction, the 70% natural frequency is 1.10 Hz, and it is nearly equal to 1.14 Hz under the bidirectional 50%-scale OS2 excitation. In the *x*-direction first mode, the assumed damping ratios of 2 and 3% are less than the average identified values in Table 5.

A comparison of Figures 12 and 14 indicates the response differences under the Kobe excitation. The case of 85–2% predicts the peak responses better than the case of 70–3% under the *x*-direction and the *y*-directions 16% excitations. The

case of 85–2% in Figure 14 can be accepted similarly to Cases X-0, X-1, Y-0 and Y-1 in Figure 12. In Figures 14 (a) and (b), the case of 70–3% predicts larger velocities and displacements than the case 85–2%. A lower frequency increased the response displacement, and this displacement tendency can be observed in all excitations. This implies that the tuning of natural frequencies was more important than the damping effect under the excitations. Under the 50%-scale excitations, the difference between the measured response and its prediction becomes more remarkable than the difference between Figures 12 and 14.

TABLE 6 Averaged prediction errors responding to Figures 12-15

Test sequential No.	Earthquake Scale Input dir.	Figures 12-13				Figures 14-15			
		x-dir.		*y*-dir.		*x*-dir.		*y*-dir.	
		Vel.	Disp.	Vel.	Disp.	Vel.	Disp.	Vel.	Disp.
1	Kobe 16% *x*-dir.	+10 +4	+8 +2	Not evaluated		+26 +46	+18 +71	Not evaluated	
2	Kobe 16% *y*-dir.	Not evaluated		+6 −4	+3 −7	Not evaluated		−6 +9	−11 +25
3	OS2 20% *y*-dir.	Not evaluated		+9 −2	+1 −8	Not evaluated		−28 −24	−36 −15
4	Kobe 50% *x*-dir.	+22 +16	+17 +11	Not evaluated		+28 +30	+15 +41	Not evaluated	
5	OS2 50% *x*- & *y*-dir.	+15 +8	+11 +6	+13 +2	+11 ±0	+22 +37	+1 +40	+1 −10	+2 −1
6	Kobe 50% *x*- & *y*-dir.	+12 +6	+9 +4	−3 −13	−1 −9	+33 +27	±0 +13	±0 −6	−12 −8

Figures 12 & 13: Upper line for Cases X-0 or Y-0, Lower for Cases X-1 or Y-1
Figures 14 & 15: Upper line for 85%−2%, Lower for 70%−3%

A comparison of Figures 13 and 15 indicates response differences under OS2 excitations. Under the *y*-directional 20%-scale excitation, the case of 70–3% predicts the peak displacement responses better than the case of 85–2%. The stiffness softening in the first storey makes it difficult to predict the seismic responses under 50% scale excitations. However, the prediction accuracy is better under the 50%-scale OS2 excitation than under the 50%-scale Kobe excitation because this method assumes that the identified mode shapes will not change under the coming earthquake, and the local damage affects the global seismic response of the structure under the OS2 excitations less than under the Kobe excitations.

Table 6 summarises the averaged errors in the prediction in response to Figures 12–15. In the columns of Figures 12 and 13, the upper lines indicate Cases X-0 or Y-0, and the lower lines indicate Cases X-1 or Y-1. In the columns of Figures 14 and 15, the upper lines indicate 85% natural frequency with 2% damping ratio (85–2%) and the lower lines indicate 70% natural frequency with 3% damping ratio (70–3%). From the four figures and the table, a better prediction can be found under (1) Cases X-1 and Y-1 similar to Cases X-0 and Y-0, (2) 16%- and 20%-scale excitations (compared to 50%-scale excitations), (3) the condition that the single-input-single-output system identification is possible (Figures 12 and 13 compared to Figures 14 and 15), and (4) OS2 excitations (compared to Kobe excitations).

As described in Section 1, References 20, 28, 29, and 30 verified the proposed prediction methods for high-rise buildings based on the fact that the accuracy of the predictions is within an error of 20% for the maximum response at each floor. This study also exhibited nearly the same level of error. The proposed method can estimate the peak accelerations, velocities, and displacements at the microtremor locations. By considering specifications of the structural and non-structural components and the past seismic structural damages, the building owners can temporally assess the seismic damages soon after seismic events. Peak response information with 20% error can be considered acceptable for checking if buildings are safe for reoccupation or not after a significant earthquake.

6. CONCLUSIONS

The applicability of the proposed modelling was studied through shaking-table tests of a 4-storey steel specimen structure. An equation of motion was modelled for an M-DOF linear building based on microtremor measurements. The first advantage of the proposed approach is that it can obtain seismic responses at microtremor sensor locations without information about the mass, damping, and stiffness matrices. It means that the model does not need any structural design documents to estimate peak responses that are linked with seismic damages of structural and non-structural components. Compared to the past methods, the second advantage is that the modelling is unconstrained by structural shape, composition of frames, connections of structural members, and the assumption of a rigid floor. Increasing the number of microtremor sensor locations produces a detailed structural model with more lumped masses. The third advantage is that the seismic response estimation needs at least one sensor to measure seismic input accelerations and to estimate seismic responses. The seismic response prediction considers actual model properties of a building. The main conclusions of this study are summarised below.

(1) The proposed method demands that the natural frequencies of the structure be identified in several lower vibration modes based on microtremor measurements; the corresponding modal amplitudes are identified at the sensor

locations to record the microtremor. The key process is evaluating the participation vector for input earthquakes by considering a limited number of identified modes. The application identifies the mode truncation error in the modal analysis.

(2) Before the shaking-table tests, the microtremor was recorded at 15 locations with five accelerometers in the 4-storey steel test structure. The reference sensor location is used to integrate the local mode shapes obtained independently from the four measurements into the global mode shapes of the specimen. The natural frequencies and mode shapes are identified by the FDD method. The approximated participation vectors depend on the selection of the identified modes and the sensor locations used. Thus, it is the best for the structure to consider all identified modes with the selection of sensor locations on the upper floors, because the mode truncation errors appear at the lumped masses near the base.

(3) To understand the dynamic property changes of the structure with different scales of ground motions, the modal identification by the recursive LSM method with a forgetting factor was applied to the recorded accelerations under the shaking-table tests. The dominant natural frequencies decreased and modal amplitudes at the second and third floors increased in response to the repetitions of shaking-table tests with an increase in the excitation scales.

(4) The applicability of the proposed approach was first studied by updating the natural frequencies and damping ratios obtained from microtremors with those obtained from the shaking-table tests. Next, we considered the standard assumptions for the structural designs in Japan. The prediction accuracy is best when the participation vector for seismic input is obtained from sensors located on the upper floors; the structure mostly exhibits elastic response; a modal system identification is applied to the seismic measurement; and local damage does not affect the global seismic response of the structure. The reason is that this method assumes that identified mode shapes do not change due to the occurrence of an earthquake. On the contrary, this limited ability may be useful for the building owners and users from a viewpoint of structural health monitoring because in the event of a strong nonlinear case, they can find out damages of structural and non-structural component with their naked eyes directly.

(5) Further applicability studies are expected because the simple shape of the test specimen does not take the advantage that the modelling is unconstrained by structural shape and rigid floor assumption.

ACKNOWLEDGEMENTS

This work was supported by JSPS KAKENHI (Grant Number 20K05027) and by the Tokyo Metropolitan Resilience Project of the National Research Institute for Earth Science and Disaster Resilience. The authors greatly appreciate the financial support provided.

REFERENCES

1. Steel Committee of Kinki Branch, Architectural Institute of Japan. Reconnaissance report on damage to steel building structures observed from the 1995 Hyogoken-Nanbu (Hanshin/Awaji) Earthquake (Abridged English Edition). 1995. http://news-sv.aij.or.jp/kinki/activity/research/s_struct/tekkotu-e.pdf. Steel Committee of Kinki Branch, Architectural Institute of Japan.
2. Sekiya N, Hiroi U. The Problem of stranded commuters in metropolitan area in the East Japan Great Earthquake, *Journal of Japan Society for Safety Engineering* 2011, 50(6): 495-500 (in Japanese).
3. Japan Cabinet Office. Guidelines for people who have difficulty returning home after an large earthquake (translated by authoers). 2015, http://www.bousai.go.jp/jishin/kitakukonnan/pdf/kitakukonnan_guideline.pdf (in Japanese). Cabinet Office, Government of Japan.
4. Tokyo Metropolitan. Handbook for people who have difficulty returning home in Tokyo (translated by authors). 2020, https://www.bousai.metro.tokyo.lg.jp/_res/projects/default_project/_page_/001/001/369/202008.pdf (in Japanese). Tokyo Metropolitan Government.
5. Osaka Prefecture Government. Guidelines for people who have difficulty returning home in Osaka after an large earthquake https://www.pref.osaka.lg.jp/attach/23998/00000000/chirashi.pdf (in Japanese). Osaka Prefecture Government.
6. Fujino Y, Siringoringo DM, Ikeda Y, Nagayama T, Mizutani T. Research and implementations of structural monitoring for bridge and building structures in Japan, *Engineering* 2019;5(6):1093-1119.
7. Limongelli MP. Optimal location of sensors for reconstruction of seismic responses through spline function interpolation. *Earthquake Eng. Struct. Dyn.* 2003;32(7):1055-1074.
8. Kabe AM. Stiffness matrix adjustment using mode data. *AIAA J.* 1985;23(9):1431-1436.
9. Fahrat C, Hemez F. Updating finite element dynamic models using an element-by-element sensitivity methodology. *AIAA J.* 1993;31(9):1702-1711.
10. Yang CD, Yeh FB. Identification, reduction and refinement of model parameters by eigensystem realization algorithm. *J. Guid. Control Dyn.* 1990;13(6):1051-1059.
11. Hoshiya M, Saito E. Structural identification by extended Kalman filter. *J. Eng. Mech.* 1984;110(12):1757-1770.
12. Hoshiya M, Sutoh A. Kalman Filter-Finite element method in identification. *J. Eng. Mech.* 1993;119(2):197-210.
13. Shi ZY, Law SS, Zhang LM. Damage detection by directly using incomplete mode shapes. *J. Eng. Mech.* 1999;126(6): 656-660.
14. Law SS, Shi ZY, Zhang LM. Structural damage detection from incomplete and noisy modal test data. *J. Eng. Mech.* 2000;124(11):1280-1288.
15. Levine-West M, Milman M, Kissil A. Mode shape expansion techniques for prediction. *Proc. First World Conf. Struct Control* 1994, IASC, Los Angeles, USA; 2: TA3 33-42.
16. Shah PC, Udwadia FE. A methodology for optimal sensor locations for identification of dynamic systems. *J. Appl. Mech.* 1978;45(1):188-196
17. Udwadia FE. Methodology for optimum sensor locations for parameter identification in dynamic systems. *J. Eng. Mech.* 1994;120(2):368-390.
18. Heredia-Zavoni E, Esteva L. Optimal Instrumentation of uncertain structural systems subject to earthquake ground motions.

Earthquake Eng. Struct. Dyn. 1998;27(4):343-362.
19. Heredia-Zavoni E, Montes-Iturrizage R, Esteva L. Optimal instrumentation of structures on flexible base for system identification. *Earthquake Eng. Struct. Dyn*. 1999;28(12):1471-1482.
20. Ikeda Y, Hisada Y. Earthquake responses on all floors in a building estimated by observation records on some restricted floors, *J. Jap. Assoc. Earthquake Eng.* 2013;13(4):38-54 (in Japanese)
21. Ikeda Y, Kurata M. A multi-degree-of-freedom building model based on microtremor measurement for seismic response estimation. *Annual Meeting* 2019, *Disaster Prevention Research Institute*, *Kyoto Univ.*; Kyoto, Japan: 2 pages, Article ID B04, https://www.dpri.kyoto-u.ac.jp/hapyo/19/pdf/B04.pdf. (in Japanese)
22. Xie J, Ikeda Y, Kurata M. Multi-degree-of-freedom linear building model based on microtremor measurement for seismic response analysis. *J. Struct. Eng.*, *Arch. Inst. Jap*. 2021;67B:509-518. (in Japanese)
23. Del Gobbo GM, Williams M, Blakeborough A. Seismic performance assessment of a code compliant multistorey building. ICUR 2016 *Int. Conf. on Urban Risks*, Lisbon, Portugal: 237-244.
24. Derakhshan H, Walsh KQ, Ingham JM, Griffith MC, Thambiratnam DP. Seismic fragility assessment of nonstructural components in unreinforced clay brick masonry buildings. *Earthquake Eng. Struct Dyn.* 2019;1-16.
25. Lee TH, Kato M, Matsumiya T, Suita K, Nakashima M. Seismic performance evaluation of non‐structural components: drywall partitions. *Earthquake Eng. Struct. Dyn.* 2007; 36(3):367-382.
26. Otsuki Y, Kurata M, Skalomenos KA, Ikeda Y. Damage sequence and safety margin assessment of expansion joints by shake table testing. *Earthquake Eng. Struct. Dyn.* 2019; 48(1):3-26.
27. Petrone C, Magliulo G, Manfredi G. Seismic demand on light acceleration-sensitive nonstructural components in European reinforced concrete buildings. *Earthquake Eng. Struct. Dyn.* 2015; 44(8):1203-1217.
28. Hatada T, Ikeda Y, Hagiwara H, Nitta Y, Nishitani A. Damage evaluation method based on acceleration measurement on some restricted floors, *Proc. 16th Eur. Conf. Earthquake Eng.* 2018; Thessaloniki, Greece: 12 pages, Article ID 10305.
29. Morii T, Okada K, Shiraishi M, Sugimoto K, Terada T, Sato T, Tobita J. Seismic response estimation of whole building based on limited number of acceleration records for structural health monitoring system shortly after an earthquake: System application for large shaking-table test of an 18 story steel building. *J. Struct. Constr. Eng. (Trans. AIJ)* 2016; 81:2045-2055. (in Japanese)
30. Kodera K, Nishitani A, Okihara Y. Cubic spline interpolation-based estimation of all story seismic responses with acceleration measurement at a limited number of floors. *Jap. Arch. Rev.* 2020; 3(4):435-444.
31. Xie J, Ikeda Y, Kurata M. Modal identification of large-scale low-rise buildings through microtremor measurements, *Proc. 17th World Conf. on Earthquake Eng.* 2021; Sendai, Japan: 12 pages, Paper ID 3b-0015.
32. ICC IBC-2021 (International Building Code 2021), International Code Council. 2021.
33. EN 1998 (Eurocode 8: Design of structures for earthquake resistance), European Committee for Standardization. The European Union. 2004.
34. The Building Standard Law of Japan, The Building Center of Japan (BCJ). 2016.
35. Wenzel H, Picher D. Ambient Vibration Monitoring. John Wiley & Sons, West Sussex, England. 2005.
36. Suzuki K. A study on problems of load combination in a seismic design. *Comprehensive Urban Studies*, *Tokyo Metropolitan Univ.* 1983; 20: 181-192. https://www.ues.tmu.ac.jp/cus/archives/cn17/pdf/20-12.pdf. (in Japanese)
37. Kurata M, *et al*. E-Defense shake table test of steel hospital building: Part I Test plan. *Summary for AIJ Annual Meeting* 2021; Structure II: Article ID 21485, 969-970. (In Japanese)
38. Brincker R, Zhang L, Andersen P. Modal identification from ambient responses using frequency domain decomposition. *Proc. 18th Int. Modal Analysis Conf.* 2000; San Antonio, Texas, USA; 625-630.
39. Kahlig P. Some aspects of Julius von Hann's contribution to modern climatology, Interactions between Global Climate Subsystems: The Legacy of Hann, Geophysical Monograph Series 75, American Geophysical Union, 1993: 1-7.
40. Gentile C. Saisi A. Ambient vibration testing of historic masonry towers for structural identification and damage assessment, *Const. Build. Mater.* 2007; 21:1311–1321.
41. Jeary AP. Damping in tall buildings: A mechanism and a predictor. *Earthquake Eng. Struct. Dyn.* 1986; 14:733-750.
42. Loh CH, Lin HM. Application of off-line and on-line identification techniques to building seismic response data, *Earthquake Eng. Struct. Dyn.* 1996; 25: 269-290.
43. Ljung L, Söderström T. Theory and Practice of Recursive Identification, MIT press, Cambridge, Mass. 1983.
44. Ikeda Y. Verification of system identification utilizing shaking-table tests of a full-scale 4-story steel building, *Earthquake Eng. Struct. Dyn.* 2016; 45:543–562
45. Çelebi M, Şafak E. Seismic response of Transamerica building. I: Data and preliminary analysis. *J. Struct. Eng.* 1991; 117(8): 2389-2404.
46. Çelebi M, Şafak E. Seismic response of Pacific Park Plaza. I: Data and preliminary analysis. *J. Struct. Eng.* 1992; 118(6): 1547-1565.
47. Çelebi M, Liu HP. Before and after retrofit–response of a building during ambient and strong motions. *J. Wind Eng. Industrial Aerodyn.* 1998; 77: 259-268.
48. Çelebi M, Phan LT, Marshall RD. Dynamic characteristics of five tall buildings during strong and low-amplitude motions. *The structural design of tall buildings* 1993; 2(1): 1-15.
49. Kohler MD, Davis PM, Şafak E. Earthquake and ambient vibration monitoring of the steel-frame UCLA Factor building. *Earthquake Spectra* 2005; 21(3): 715-736.
50. Dunand F, Bard P, Rodgers J. Comparison of the dynamic parameters extracted from weak, moderate and strong motion recorded in buildings. 1st European Conf. on Earthquake Eng. and Seismology 2006, Geneva, Switzerland, 3-8, Paper ID: 1021
51. Dunand F, Rodgers JE, Acosta AV, et al. Ambient vibration and earthquake strong-motion data sets for selected USGS extensively instrumented buildings. US Geological Survey. Open-File Rept. 2004-1375, 2004.
52. Çelebi M, et al. Responses of two tall buildings in Tokyo, Japan, before, during, and after the M9. Tohoku Earthquake of 11 March 2011. *Earthquake Spectra* 2016; 32(1): 463-495.